

Use of Fluorescent-Protein Tagging To Determine the Subcellular Localization of *Mycoplasma pneumoniae* Proteins Encoded by the Cytadherence Regulatory Locus

Tsuyoshi Kenri,^{1*} Shintaro Seto,^{2,†} Atsuko Horino,¹ Yuko Sasaki,¹
Tsuguo Sasaki,¹ and Makoto Miyata^{2,3}

Department of Bacterial Pathogenesis and Infection Control, National Institute of Infectious Diseases, Musashimurayama, Tokyo,¹ and Department of Biology, Graduate School of Science, Osaka City University,² and PRESTO, JST,³ Sumiyoshi-ku, Osaka, Japan

Received 13 May 2004/Accepted 15 July 2004

Mycoplasma pneumoniae lacks a cell wall but has internal cytoskeleton-like structures that are assumed to support the attachment organelle and asymmetric cell shape of this bacterium. To explore the fine details of the attachment organelle and the cytoskeleton-like structures, a fluorescent-protein tagging technique was applied to visualize the protein components of these structures. The focus was on the four proteins—P65, HMW2, P41, and P24—that are encoded in the *crl* operon (for “cytadherence regulatory locus”), which is known to be essential for the adherence of *M. pneumoniae* to host cells. When the P65 and HMW2 proteins were fused to enhanced yellow fluorescent protein (EYFP), a variant of green fluorescent protein, the fused proteins became localized at the attachment organelle, enabling visualization of the organelles of living cells by fluorescence microscopy. The leading end of gliding *M. pneumoniae* cells, expressing the EYFP-P65 fusion, was observed as a focus of fluorescence. On the other hand, when the P41 and P24 proteins were labeled with EYFP, the fluorescence signals of these proteins were observed at the proximal end of the attachment organelle. Coexpression of the P65 protein labeled with enhanced cyan fluorescent protein clearly showed that the sites of localization of P41 and P24 did not overlap that of P65. The localization of P41 and P24 suggested that they are also cytoskeletal proteins that function in the formation of unknown structures at the proximal end of the attachment organelle. The fluorescent-protein fusion technique may serve as a powerful tool for identifying components of cytoskeleton-like structures and the attachment organelle. It can also be used to analyze their assembly.

Mycoplasma pneumoniae, one of the smallest self-replicating bacteria known, is a causative agent of bronchitis and primary atypical pneumonia in humans (43, 44). *M. pneumoniae* lacks a cell wall and hence has a pleomorphic cell shape. However, a majority of *M. pneumoniae* cells in cultures are filamentous and have a differentiated terminal structure at one pole. This terminal structure, the attachment organelle, is a tapered membrane protrusion responsible for the adherence of *M. pneumoniae* to host respiratory epithelium (cytadherence) (23, 24). The attachment organelle renders *M. pneumoniae* cells asymmetric and functions as a leading end for gliding motility. This organelle also may have a role in initiating cell division in *M. pneumoniae*, because the bifurcation of the attachment organelle seems to occur prior to the binary fission of *M. pneumoniae* (2, 6, 7, 25, 26, 34, 36, 48).

The attachment organelle and polar filamentous cell shape of *M. pneumoniae* are thought to be stabilized by intracellular cytoskeleton-like structures, which have been observed in electron micrographs of *M. pneumoniae* (5, 25, 33). The most remarkable architectural feature of the cytoskeleton-like structures is the electron-dense core, a rod-like structure that exists

longitudinally at the center of the attachment organelle (33). This rod-like structure, measuring about 300 nm long and 80 nm thick, has a knob at the distal end (terminal button) (33, 45). A network of fibrous structures is also observed in the cytoplasm of *M. pneumoniae* (33). These cytoskeleton-like structures are major components of the Triton X-100-insoluble fraction of *M. pneumoniae* cells (Triton shell) and are thought to have a scaffold-like function upon which other cell components construct *M. pneumoniae* cells (45, 51).

A recent report indicated that the Triton X-100-insoluble fraction contains about 100 proteins, including most of the known proteins required for cytadherence (P1, B, C, HMW1, HMW2, and HMW3) (45). These cytadherence-related proteins are believed to be the main components of the attachment organelle and are encoded in three operons, designated *p1*, *hmw*, and *crl*, in the genome (24, 25). Protein P1 (encoded in the *p1* operon) is a major adhesin molecule responsible for cytadherence and is densely clustered at the surface of the attachment organelle (9, 18, 26, 48). Proteins B, C, HMW1, HMW2, and HMW3, called cytadherence accessory proteins, are not adhesin molecules but are required for the formation of functional attachment organelles (2, 3, 25). Proteins B and C, also named P90 and P40 (2, 26), are products of open reading frame 6, which exists just downstream of the *p1* gene in the *p1* operon (19). Proteins B and C associate with protein P1 at the attachment organelle and may support the proper structural configuration of P1 (29, 30). HMW1, HMW2, and HMW3 are large proteins necessary for the localization of P1

* Corresponding author. Mailing address: Department of Bacterial Pathogenesis and Infection Control, National Institute of Infectious Diseases, 4-7-1 Gakuen, Musashimurayama, Tokyo 208-0011, Japan. Phone: 81-42-561-0771. Fax: 81-42-565-3315. E-mail: kenri@nih.go.jp.

† Present address: Department of Oral Microbiology, Meikai University School of Dentistry, 1-1 Keyakidai, Sakado, Saitama 350-0283, Japan.

at the attachment organelle. These HMW proteins are present in high concentrations at the attachment organelle and are thought to be the most likely components of the electron-dense core (3, 25, 48, 49, 52). HMW1 and HMW3 are encoded in the *hmw* operon, and the gene encoding HMW2 is in the *crl* operon (24). In addition to these cytoadherence-related proteins, the Triton X-100-insoluble fraction contains proteins P65 and P200. P65 and P200 share a structural domain, the acidic proline-rich domain, with HMW1 and HMW3 (40, 41). The structural similarity suggests that proteins P65 and P200 have roles similar to those of HMW1 and HMW3 as components of cytoskeleton-like structures. However, it is not clear whether proteins P65 and P200 participate in cytoadherence. Recent studies revealed that P65 localizes to the attachment organelle with P30, an additional adhesin protein that is an essential factor for cytoadherence (2, 20, 25, 48, 49). The genes encoding P65 and P30 are located in the *crl* and *hmw* operons, respectively. The gene encoding P200 is not located in one of the three operons of cytoadherence-related proteins (2, 24).

Although these candidate components of the attachment organelle and cytoskeleton-like structures have been identified, the spatial configuration and interaction between these proteins are poorly understood. Antibodies have been used to localize specific proteins to the attachment organelle (46, 48, 49, 52), but their use is limited because of the need for specificity of an antibody for a target protein and the inability to observe living systems in real time. Green fluorescent protein (GFP), an intrinsically fluorescent molecule obtained from the jellyfish *Aequorea victoria*, is widely used to study protein-protein interactions, cell division, and gene expression in a variety of organisms in real time (39, 50). In this study, we developed a dual GFP expression system for *M. pneumoniae* to study the spatial relationship of P65 to HMW2, P41, and P24, which are encoded in the *crl* operon (28).

MATERIALS AND METHODS

Organism and culture conditions. The *M. pneumoniae* strains listed in Table 1 were cultured in PPLO medium (2.1% PPLO broth [Becton Dickinson, Sparks, Md.], 0.25% glucose, 0.002% phenol red, 0.5% yeast extract [Becton Dickinson], 10% horse serum [Gibco BRL, Rockville, Md.], 50 µg of ampicillin/ml) or in Aluotto medium (1, 38) at 37°C. For drug-resistant *M. pneumoniae* strains, 18 µg of gentamicin/ml or 15 µg of chloramphenicol/ml was added to the media. *Escherichia coli* JM83 (53), DH5α (13), and DB3.1 (Invitrogen, Carlsbad, Calif.) were used as host strains to construct plasmids and were grown in Luria-Bertani medium (47) with or without 50 µg of ampicillin/ml, 50 µg of kanamycin/ml, and 15 µg of chloramphenicol/ml at 37°C.

Construction of fusion genes and plasmids. The synthetic oligonucleotides used for plasmid construction are listed in Table 2. *M. pneumoniae* M129 genomic DNA was prepared by a conventional phenol extraction method. The *p65* gene was amplified from the genomic DNA by PCR with primers P65F-Bam and P65R-Nco. To minimize mutations caused by PCR amplification, high-fidelity DNA polymerase PyroBest (Takara, Tokyo, Japan) was used. The amplified fragment was digested with BamHI and NcoI and was inserted into the BamHI-NcoI site (the 5' end of the *eyfp* gene) of plasmid pEYFP (Clontech, Palo Alto, Calif.), producing a plasmid that we designated pTK150. The *p65* gene was also amplified from the genomic DNA by PCR with primers P65F-Bsr and P65R-Eco. The amplified fragment was inserted into the BsrGI-EcoRI site (the 3' end of the *eyfp* gene) of plasmid pEYFP after digestion with BsrGI and EcoRI, producing a plasmid that we designated pTK153. The *p65-eyfp* and *eyfp-p65* fusion genes were excised from plasmids pTK150 and pTK153 by using PvuII and StuI and were inserted into the SmaI site of plasmid pISM2062.2 (22), producing plasmids pTK155 and pTK158, respectively (Table 3). Plasmids pTK161 and pTK162 (Table 3) were constructed by replacing the *E. coli lac* promoter sequence in pTK158 (derived from plasmid pEYFP) with *p65* or *tuf* promoter

TABLE 1. *M. pneumoniae* strains used in this study^a

Strain	Description ^b
M129	Wild type
TK2062	M129(pISM2062.2)
TK155	M129(pTK155)
TK161	M129(pTK161)
TK162	M129(pTK162)
TK164	M129(pTK164)
TK165	M129(pTK165)
TK210	M129(pTK210)
TK2100	TK210(pISM2062.2)
TK2310	TK210(pMPN310)
TK2311	TK210(pMPN311)
TK2312	TK210(pMPN312)
TK2310T	TK210(pMPN310-tuf)
TK2311T	TK210(pMPN311-tuf)
TK2312T	TK210(pMPN312-tuf)
TK3310	M129(pMPN310)
TK3311	M129(pMPN311)
TK3312	M129(pMPN312)
TK3310T	M129(pMPN310-tuf)
TK3311T	M129(pMPN311-tuf)
TK3312T	M129(pMPN312-tuf)

^a All strains were designed in this study, except for the wild-type strain (31).

^b Tn4001 plasmids were used to transform *M. pneumoniae*.

fragments from *M. pneumoniae* at the BamHI-NcoI site. The *p65* and *tuf* promoter fragments were obtained from *M. pneumoniae* genomic DNA by PCR with primers P65F-Bam and P65-PR and primers tuf-PF and tuf-PR, respectively. These promoter fragments were also used to replace the *p65* gene and its promoter sequence in pTK155 at the BamHI-NcoI site. The resulting plasmids, which expressed the *eyfp* gene alone from the *p65* and *tuf* promoters, were designated pTK164 and pTK165, respectively (Table 3).

The *ecfp* gene was amplified from plasmid pECFP (Clontech) by PCR with primers CFP1F-Sma and CFP-R. The amplified *ecfp* fragment was inserted into the SmaI site of pKV104, producing a plasmid that we designated pTK205. pKV104 contains a chloramphenicol-resistant (Cm^r) variant of Tn4001 (12) and was kindly provided by D. C. Krause of the University of Georgia. The *lac* promoter region of pTK205 (upstream of the *ecfp* gene) was replaced at the SmaI-AgeI site with the *M. pneumoniae tuf* promoter sequence amplified by PCR with primers tuf-F and tufR-Age, resulting in plasmid pTK207. The BsrGI site of pTK207 (the 3' end of the *ecfp* gene) was converted to an EcoRV site with an oligonucleotide linker, 160RVS. Next, the Gateway vector conversion system (reading frame cassette A) (Invitrogen) was inserted into the EcoRV site, producing a plasmid that we designated pTK207-D. The *p65* gene was amplified from *M. pneumoniae* genomic DNA with primers MPN309-F-Gw and MPN309-R-Gw, subcloned into plasmid pDONR201 (Invitrogen) by using BP clonase (Invitrogen), and then transferred to plasmid pTK207-D by using LR clonase (Invitrogen); this procedure produced plasmid pTK210 (Table 3).

Plasmids containing *hmw2*, *p41*, and *p24* fusion genes were constructed as follows. The BsrGI site of plasmid pTK164 and that of plasmid pTK165 were converted to an EcoRV site by inserting an oligonucleotide linker, 160RVS. Next, the Gateway vector conversion system (reading frame cassette A) was inserted in the created EcoRV site, producing plasmids pTK164-D and pTK165-D. The *hmw2* gene sequence was amplified from *M. pneumoniae* genomic DNA by PCR with primers MPN310-F-Not and MPN310-R-Asc. After digestion with NotI and AscI, the *hmw2* gene fragment was inserted into the NotI-AscI site of plasmid pENTR/D-TOPO (Invitrogen), resulting in a plasmid that we designated pMPN310-E. The *p41* and *p24* gene sequences were amplified from *M. pneumoniae* genomic DNA by PCR with primers MPN311-F-Gw and MPN311-R-Gw and primers MPN312-F-Gw and MPN312-R-Gw, respectively. The amplified fragments were subcloned into plasmid pDONR201 by using BP clonase, producing plasmids that we designated pMPN311-E and pMPN312-E. The *hmw2*, *p41*, and *p24* gene fragments of plasmids pMPN310-E, pMPN311-E, and pMPN312-E were transferred to plasmids pTK164-D and pTK165-D by using LR clonase. The resulting plasmids (pMPN and pMPN-tuf series), which are listed in Table 3, were used to transform *M. pneumoniae*.

Transformation of *M. pneumoniae*. *M. pneumoniae* with the modified Tn4001 (Tn4001mod) plasmids was transformed by the electroporation method described by Hedreyda et al. (15). The transformed cells were grown in liquid PPLO medium containing 18 µg of gentamicin/ml or 15 µg of chloramphenicol/

TABLE 2. Synthetic oligonucleotides used in this study

Oligonucleotide	Sequence ^a
P65F-Bam.....	<u>GCGGGATCCTGCAGCAGCTGACAACAACATTTAGCACACT</u>
P65R-Nco.....	<u>CTAGCCATGGCTTCGTAAAATTCATCACCAC</u>
P65F-Bsr.....	<u>GAGCTGTACAAGATGGATATAAATAAACCAGG</u>
P65R-Eco.....	<u>TCGCGGAATTCAGCTGTTTATTTCGTAAAATTCATCACCAC</u>
P65-PR.....	<u>CAACCCATGGCATTATATCCATTTACTGTCT</u>
tuf-PF.....	<u>GTGGGATCCATTTTGCAAACCTGATGACAA</u>
tuf-PR.....	<u>TAACCATGGGTTTAGATCGGTCAAATTT</u>
CFPIF-Sma.....	<u>GATCCCGGGAGCGCCCAATACGCAAACCGCC</u>
CFP-R.....	<u>CCTATTATTTTGGACACCAGAC</u>
165RVS.....	<u>GTACGATATC</u>
tuf-F.....	<u>ATTTTGCAAACCTGATGACAA</u>
tufR-Age.....	<u>TCGGACCGGTTTCTCTCTTGCCATGTGTTTG</u>
MPN309-F-Gw.....	<u>GGGGACAAGTTTGTACAAAAAAGCAGGCTTCATGGATATAAATAAACCAGGTTGAA</u>
MPN309-R-Gw.....	<u>GGGGACCACTTTGTACAAGAAAGCTGGGTTATTATTTCGTAAAATTCATCACCAC</u>
MPN310-F-Not.....	<u>CCGCGGCCGCCATGAATGATACTGACAAGAAGT</u>
MPN310-R-Asc.....	<u>GTCGGCGGCCCTTATTAGCTGCTTTTGGGC</u>
MPN311-F-Gw.....	<u>GGGGACAAGTTTGTACAAAAAAGCAGGCTTCATGACTAATGATTACCAACAATTTAAA</u>
MPN311-R-Gw.....	<u>GGGGACCACTTTGTACAAGAAAGCTGGGTATCCTTCATTACTTTGTTCT</u>
MPN312-F-Gw.....	<u>GGGGACAAGTTTGTACAAAAAAGCAGGCTTCATGAAGGATAGTGCACCTAACACT</u>
MPN312-R-Gw.....	<u>GGGGACCACTTTGTACAAGAAAGCTGGGTTACTTCTTGTAAGAAATTAAC</u>

^a Recognition sites for restriction enzymes and the *att* sites for recombinase are underlined.

ml. The transformation efficiencies were checked by counting the transformant colonies on PLO agar plates. To minimize the positional effect of Tn4001 insertion in the comparisons of the transformants, we analyzed and compared the transformant strains as a whole transformed population without picking up a single colony.

Protein analysis. *M. pneumoniae* cells were grown in tissue culture flasks to the mid-log phase and were scraped from the bottom of the flasks. The cells were collected by centrifugation at 20,000 × g for 15 min at 4°C and washed three times with phosphate-buffered saline. The final cell suspension, adjusted to a total protein concentration of 1 μg/μl, was lysed by adding sample loading buffer and was subjected to sodium dodecyl sulfate (SDS)-polyacrylamide gel electrophoresis (PAGE) at a load of 5 or 10 μg of total protein per lane (47). For Western blot analysis, the separated proteins were transferred to a nitrocellulose

membrane (Bio-Rad, Hercules, Calif.). Monoclonal antibody JL-8 (specific for *A. victoria* GFP variants) (Clontech) was used at a 1:2,000 dilution to detect enhanced yellow fluorescent protein (EYFP) and enhanced cyan fluorescent protein (ECFP). Anti-P65 antiserum (49) was also used at a 1:2,000 dilution. The reacting antibodies were detected with an alkaline phosphatase-conjugated second antibody (goat anti-mouse immunoglobulin G) (Promega, Madison, Wis.) and 5-bromo-4-chloro-3-indolylphosphate (BCIP)-nitroblue tetrazolium (NBT) color development substrate (Promega) according to manufacturer instructions.

Microscopy. *M. pneumoniae* strains were cultured in Aluotto medium at 37°C to the mid-log phase. Cytadherence-positive cells were scraped from the bottom of the culture flasks after the medium was replaced with a volume of fresh medium that was two to five times smaller. The cell suspension was passed through a 25-gauge needle several times, filtered through a membrane filter unit

TABLE 3. Plasmids constructed in this study^a

Plasmid	Vector	Marker	Promoter	Gene	Expression ^b	Fluorescence ^c	Localization ^d
pTK150	pEYFP	Ap ^r	<i>p65</i>	<i>p65-eyfp</i>	NT	NT	NT
pTK153	pEYFP	Ap ^r	<i>lac</i> (<i>E. coli</i>)	<i>eyfp-p65</i>	NT	NT	NT
pTK155	pISM2062.2	Ap ^r Gm ^r	<i>p65</i>	<i>p65-eyfp</i>	+	+	+
pTK158	pISM2062.2	Ap ^r Gm ^r	<i>lac</i> (<i>E. coli</i>)	<i>eyfp-p65</i>	–	–	–
pTK161	pISM2062.2	Ap ^r Gm ^r	<i>p65</i>	<i>eyfp-p65</i>	+	+	+
pTK162	pISM2062.2	Ap ^r Gm ^r	<i>tuf</i>	<i>eyfp-p65</i>	++	++	+
pTK164	pISM2062.2	Ap ^r Gm ^r	<i>p65</i>	<i>eyfp</i>	+	+	–
pTK164-D	pISM2062.2	Ap ^r Gm ^r Cm ^r	<i>p65</i>	<i>eyfp</i>	NT	NT	NT
pTK165	pISM2062.2	Ap ^r Gm ^r	<i>tuf</i>	<i>eyfp</i>	++	++	–
pTK165-D	pISM2062.2	Ap ^r Gm ^r Cm ^r	<i>tuf</i>	<i>eyfp</i>	NT	NT	NT
pTK205	pKV104	Ap ^r Cm ^r	<i>lac</i> (<i>E. coli</i>)	<i>ecfp</i>	NT	NT	NT
pTK207	pKV104	Ap ^r Cm ^r	<i>tuf</i>	<i>ecfp</i>	++	++	–
pTK207-D	pKV104	Ap ^r Cm ^r	<i>tuf</i>	<i>ecfp</i>	NT	NT	NT
pTK210	pTK207-D	Ap ^r Cm ^r	<i>tuf</i>	<i>ecfp-p65</i>	++	++	+
pMPN310-E	pENTR/D-TOPO	Km ^r	None	<i>hmw2</i>	NT	NT	NT
pMPN311-E	pDONR201	Km ^r	None	<i>p41</i>	NT	NT	NT
pMPN312-E	pDONR201	Km ^r	None	<i>p24</i>	NT	NT	NT
pMPN310	pTK164-D	Ap ^r Gm ^r	<i>p65</i>	<i>eyfp-hmw2</i>	+	+	+
pMPN311	pTK164-D	Ap ^r Gm ^r	<i>p65</i>	<i>eyfp-p41</i>	+	+	+
pMPN312	pTK164-D	Ap ^r Gm ^r	<i>p65</i>	<i>eyfp-p24</i>	+	+	+
pMPN310-tuf	pTK165-D	Ap ^r Gm ^r	<i>tuf</i>	<i>eyfp-hmw2</i>	++	++	+
pMPN311-tuf	pTK165-D	Ap ^r Gm ^r	<i>tuf</i>	<i>eyfp-p41</i>	++	++	+
pMPN312-tuf	pTK165-D	Ap ^r Gm ^r	<i>tuf</i>	<i>eyfp-p24</i>	++	++	+

^a *M. pneumoniae* strains transformed with Tn4001 plasmids were analyzed by Western blotting and fluorescence microscopy. NT, not applicable or not tested.

^b Expression of the fusion protein in *M. pneumoniae* cells was monitored by Western blotting: +, ++, and –, moderate, strong, and no expression, respectively.

^c Fluorescence intensity was observed by microscopy: +, ++, and –, faint, strong, and no fluorescence, respectively.

^d Localization of the fusion protein at cell poles was observed by microscopy: +, present; –, absent.

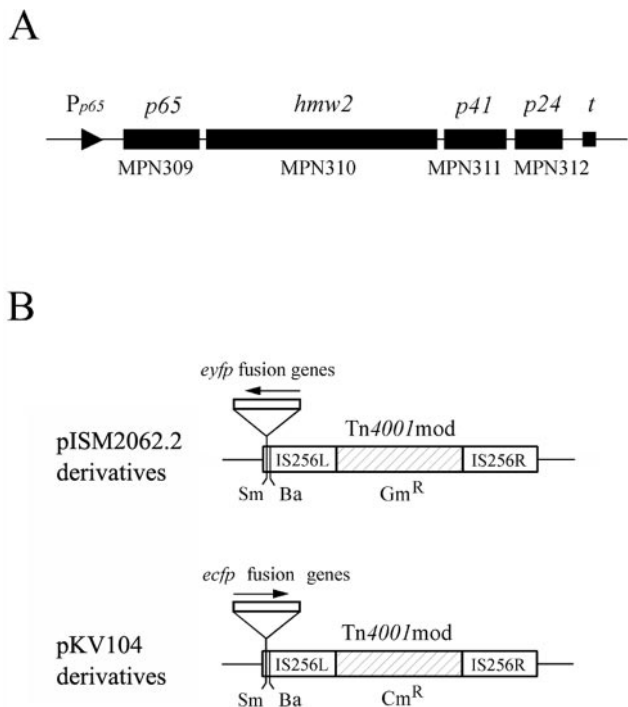


FIG. 1. (A) Schematic illustration of the *crl* operon of *M. pneumoniae*. The four rectangular bars indicate the *p65*, *hmw2*, *p41*, and *p24* genes in this operon. These genes are also designated MPN309, MPN310, MPN311, and MPN312 according to the serial numbering system of the *M. pneumoniae* genome project (8). The triangle and the square represent the *p65* promoter (P_{p65}) and the terminator (*t*) of this operon, respectively. The figure is not drawn precisely to scale. (B) Structures of modified staphylococcal transposon *Tn4001mod* vectors (11, 22). Plasmid pISM2062.2 carries a Gm^r version of *Tn4001mod*. Plasmid pKV104 carries a Cm^r version of *Tn4001mod*. The IS256L, IS256R, and drug resistance genes (Gm^r and Cm^r) of *Tn4001mod* are illustrated. Cloning sites (Sm, SmaI; Ba, BamHI) in *Tn4001mod* are indicated. The *eyfp* fusion genes were inserted into the SmaI site of pISM2062.2. The *ecfp* fusion genes were inserted into the SmaI site of pKV104. The arrows indicate the directions in which the fusion genes were inserted.

with a 0.45- μ m-pore size (Millipore, Billerica, Mass.) to disperse aggregates (46, 48), and placed on coverslips cleaned with saturated ethanolic KOH (4). The coverslips with the cell suspensions were incubated at 37°C for 0.5 to 1 h and were mounted on glass slides after excess cell suspensions were removed. To observe ECFP fluorescence, coverslips were washed twice with phosphate-buffered saline before being mounted on glass slides to reduce background fluorescence. The cells were observed with a BX51 fluorescence microscope equipped with YFP and CFP filter units (U-MYFPHQ and U-MCFPHQ, respectively) and a phase-contrast setup (Olympus, Tokyo, Japan). The images were digitized by using a Photometrics CoolSNAPcf charge-coupled device camera (Roper Scientific, Atlanta, Ga.) and LuminaVision software (Mitani Corp., Tokyo, Japan); signals were adjusted to obtain proper intensities. The fluorescence images were pseudocolored by using the LuminaVision software. The images were also processed by using Adobe Photoshop software, versions 6.0 and 7.0 (Adobe Systems, San Jose, Calif.).

To observe gliding, cells of strain TK162 were suspended in saline containing 20% horse serum. The cell suspension was inserted into a tunnel that was 12 mm wide, 18 mm long, and 0.06 mm high and that was assembled from a glass slide, a coverslip, and two pieces of double-sided tape; the cells were incubated in this tunnel for 10 min at 37°C. The cells then were observed with the fluorescence microscope at 37°C; this temperature was achieved by attaching a heating system to the sample stage and the objective lens. Cell images were recorded by using a charge-coupled device camera (WV-BP510; Panasonic, Osaka, Japan) and a digital videocassette recorder (WV-D9000; Sony, Tokyo, Japan) and were digitized as described previously (37).

RESULTS

Construction of the *p65* fusion genes and their expression in *M. pneumoniae* cells. We chose the P65 protein as the initial target for the fluorescent-protein tagging strategy by virtue of the location of its gene just downstream of the promoter of the *crl* operon (28) (Fig. 1A); this promoter can be used to express recombinant *p65* genes. The *eyfp* gene, encoding EYFP, which is a yellow-green-shifted variant of GFP that gives a stronger fluorescence emission than the wild type (10), was fused to the 3' or 5' end of the *p65* gene. The fusion genes were under the control of the native *p65* promoter and were inserted into the SmaI site of *Tn4001mod* vector plasmid pISM2062.2 (22) (Fig. 1B). The plasmids that we designated pTK155 and pTK161 carry the *p65-eyfp* and *eyfp-p65* fusion genes, respectively (Table 3). These plasmids were introduced into *M. pneumoniae* M129 by electroporation to deliver fusion genes to the chromosome by the transposition of *Tn4001mod*. Transformants TK155 and TK161 (named for plasmids pTK155 and pTK161, respectively) were obtained and were examined by fluorescence microscopy, which detected faint fluorescent signals from both strains. In most cells, the signals were located at one pole (Fig. 2), suggesting that the P65-EYFP and EYFP-P65 fusions were produced in these strains and localized at the attachment organelle. The intensities of the fluorescence signals were similar between the strains but slightly stronger in TK161 (Fig. 2).

To enhance the fluorescence intensity, we chose the *eyfp-p65* fusion gene, which exhibited slightly brighter fluorescence, and

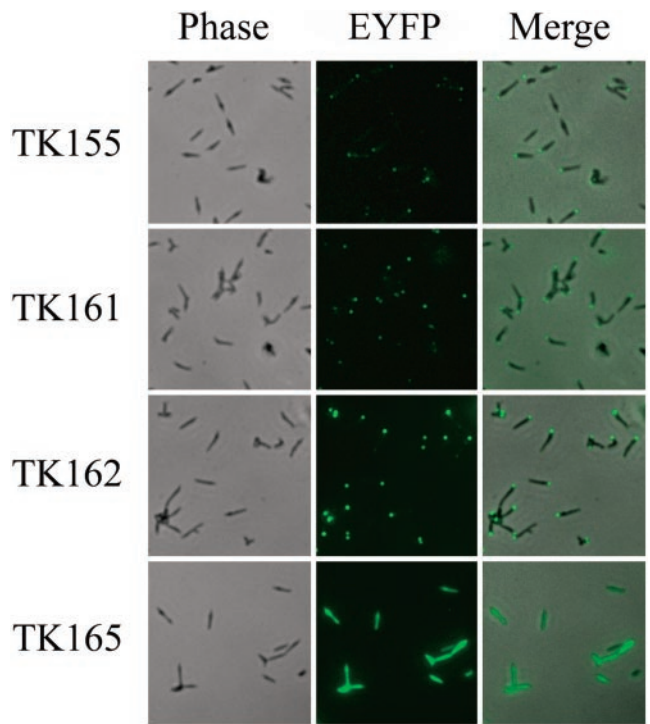


FIG. 2. Subcellular localization of EYFP fusions. The left and middle panels in each row show the same cells observed by phase-contrast microscopy and fluorescence microscopy, respectively. The right panel in each row shows the merged image of the left and middle panels. The transformants are named at left. Bar, 5 μ m.

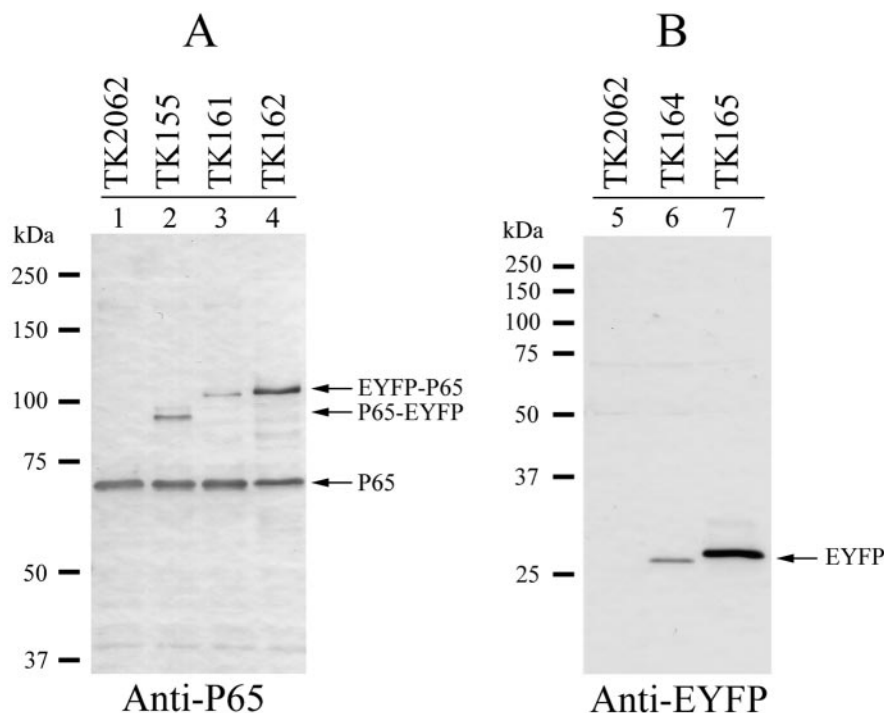


FIG. 3. Expression of fusions of P65 and EYFP in *M. pneumoniae* cells. (A) Western blot analysis of *M. pneumoniae* transformants with an anti-P65 antibody. Lysates of *M. pneumoniae* transformant cells (5 μ g of total protein) were separated by SDS-8% PAGE, transferred to a nitrocellulose membrane, and probed with an anti-P65 antibody. The positions of the detected P65-EYFP, EYFP-P65, and native P65 are indicated by arrows. Molecular sizes are shown at left. The analyzed transformants are shown above the lanes. (B) Detection of EYFP expression by Western blot analysis. Lysates of *M. pneumoniae* transformant cells (5 μ g of total protein) were separated by SDS-12% PAGE. The position of EYFP detected by an anti-EYFP (anti-GFP variant) antibody is indicated by an arrow. Molecular sizes are shown at left. The analyzed transformants are shown above the lanes.

we tested a promoter sequence of the *tuf* gene of *M. pneumoniae* instead of the *p65* promoter. Plasmid pTK162, which carries the *eyfp-p65* fusion gene under the control of the *tuf* promoter, was constructed and used to transform *M. pneumoniae* M129. The strain obtained, TK162, showed strong fluorescent signals at the cell poles (Fig. 2), suggesting higher production of the EYFP-P65 fusion in TK162 than in TK161. To confirm whether the polar localization of fusion proteins depends on the P65 moiety, we constructed plasmids pTK164 and pTK165, which carried the *eyfp* gene alone under the control of the *p65* or the *tuf* promoter (Table 3). The transformants with these plasmids, TK164 and TK165, showed fluorescence throughout the whole cell body (Fig. 2; only TK165 is shown), indicating that the polar localization of the P65-EYFP and EYFP-P65 fusions is caused by the properties of the P65 moiety. The intensity of EYFP fluorescence was strong in TK165 but faint in TK164, corresponding to their promoter activities.

We next analyzed transformant strains by Western blot analysis to examine the levels of expression of fusion proteins. By using anti-P65 antiserum, we detected P65-EYFP in TK155 and EYFP-P65 in both TK161 and TK162 (Fig. 3). TK155 and TK161 both had lower levels of fusion proteins than of native P65 (Fig. 3, lanes 2 and 3). On the other hand, the level of expression of EYFP-P65 in TK162 was comparable to that of native P65 (Fig. 3, lane 4). The size difference between P65-EYFP and EYFP-P65 (Fig. 3, lanes 2, 3, and 4) was caused by the addition of a short amino acid sequence at the N terminus

of EYFP-P65, which resulted from the construction of the promoter fusion. The anti-EYFP antibody detected EYFP in both TK164 and TK165 (Fig. 3, lanes 6 and 7). The level of EYFP was low in TK164 but high in TK165, reflecting the activities of the *p65* and *tuf* promoters. The size difference for EYFP between TK164 and TK165 was attributed to the construction of the promoter fusion. These results indicated that the fluorescence intensities of the transformants correlated with their levels of EYFP fusion expression.

The fluorescence diminished in 10 s even in TK165 cells, with the highest intensity. This rather rapid bleaching may be attributable to the small number of fluorescent molecules caused by the small dimensions of *M. pneumoniae* cells. An *M. pneumoniae* cell is about 2 μ m in length and 0.2 μ m in diameter. The total volume is estimated to be 25 times lower than that of an *E. coli* cell. The signal from the small number of fluorescent molecules may easily fall below the detection limit as a result of photobleaching of the molecules.

The cytoadherence ability of the transformants was also analyzed by a standard hemadsorption (HA) assay (14, 27). Of the colonies tested, 97% showed HA activity, suggesting that the expression of the EYFP fusions did not disturb the cytoadherence processes of *M. pneumoniae*. However, 3% of the colonies did not show HA activity. This frequency of HA-negative colonies, obviously higher than that caused by spontaneous mutation (27), may have been caused by the insertion of Tn4001 into the cytoadherence-related genes.

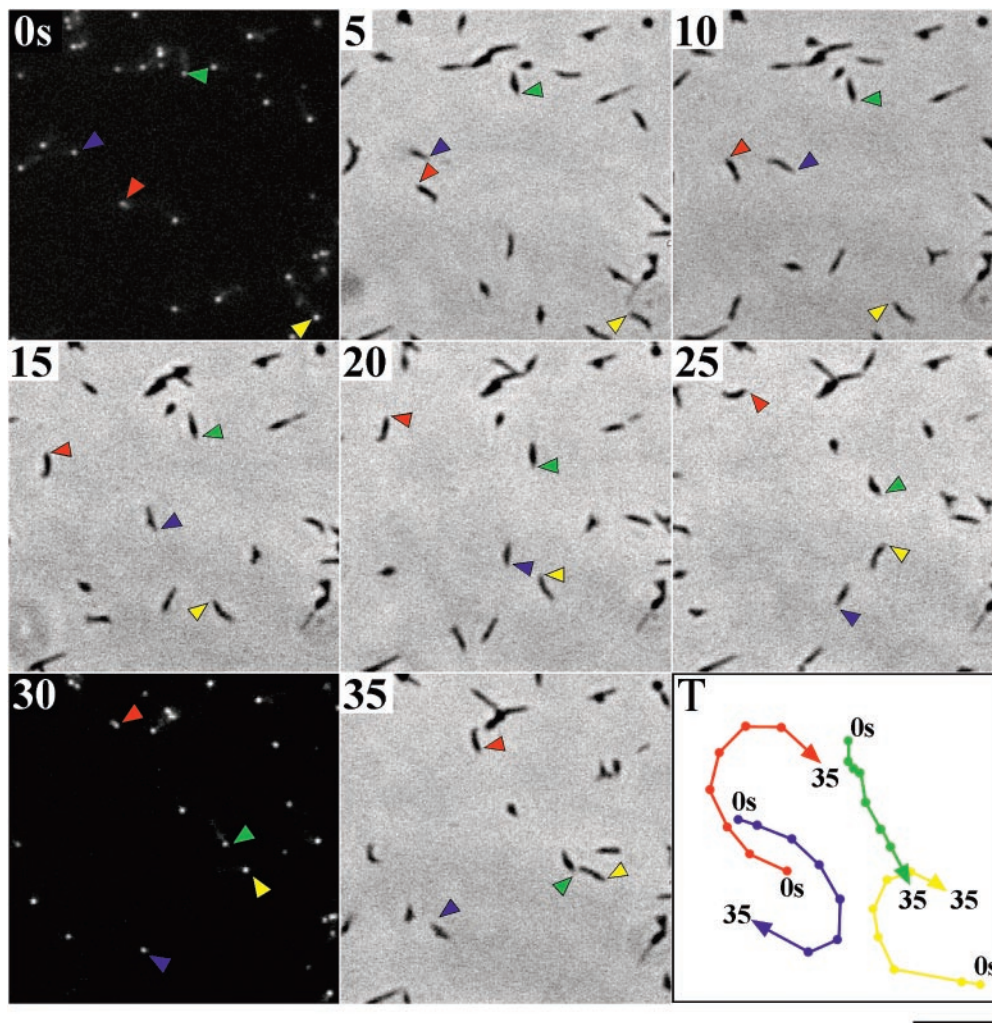


FIG. 4. Gliding motility of *M. pneumoniae* cells whose attachment organelles are fluorescently labeled with the EYFP-P65 fusion. Strain TK162 was observed by phase-contrast microscopy and fluorescence microscopy at 37°C. The phase-contrast image was recorded continuously with a video recorder. The microscope was shifted to the fluorescence setup for 2 s at 28-s intervals. The time intervals between images in this figure are 5 s. The positions of attachment organelles of four typical cells are indicated by colored arrowheads. The tracks of cell movement (positions of attachment organelles) are shown by colored lines in the bottom right panel (T). Bar, 5 µm.

Observation of gliding cells. Bredt (6, 7) and Radestock and Bredt (42) studied the gliding motility of *M. pneumoniae* cells by phase-contrast microscopy and concluded that the attachment organelle functions as the leading end of gliding cells. If EYFP-P65 fusions are properly incorporated into the attachment organelle, then the fluorescent foci must be observed at the leading end of gliding *M. pneumoniae* cells. To confirm this notion directly, we studied the gliding motility of TK162 cells, which exhibited the brightest fluorescent foci among the TK strains. To do so, we made slight modifications to a method used to observe the gliding of *Mycoplasma mobile* cells (35). TK162 cells were suspended in saline including 20% horse serum and were inserted into a tunnel assembled from a glass slide and a coverslip. We excluded heart infusion broth and yeast extract from the cell suspension, because these components of mycoplasma growth medium cause strong background fluorescence. The coverslip was maintained at 37°C on the microscope stage. Gliding cells on the glass surface and fluorescent foci were observed by phase-contrast microscopy and

fluorescence microscopy, respectively (Fig. 4). As expected, the fluorescent focus was always positioned ahead of the gliding cell, indicating the localization of EYFP-P65 at the attachment organelle. In gliding cells, the attachment organelle (fluorescent focus) always moved smoothly, while the other part of the cell body often showed lateral wobble motion, consistent with previous observations (6, 7, 42). These results suggested that the organelle kept contact with the glass surface and that the other part of the cell body detached from the surface during gliding.

The proportion of gliding cells was apparently higher in saline containing 20% serum than in growth medium (unpublished data). Nutrient-starved conditions may accelerate the movement, as observed in other gliding bacteria (32). The addition of 1 to 5% gelatin was not needed with our conditions, although it has been reported to be essential for keeping cells on the glass surface (42). This difference may be related to differences in glass surface conditions between previous studies and our investigation.

The average speed of the gliding shown in Fig. 4 was calculated to be 0.40 $\mu\text{m/s}$, consistent with previous observations (6, 21, 42). We tried multiple times to observe the cell division process of *M. pneumoniae* during 30 min of continuous video recording but failed to find cells that exhibited nascent attachment organelle formation or cytokinesis.

Subcellular localization of the HMW2, P41, and P24 proteins. We extended the fluorescent-protein tagging strategy to the other gene products of the *crl* operon (the HMW2, P41, and P24 proteins) (Fig. 1A). Although the polar localization of HMW2 at the attachment organelle was reported recently by Balish et al. (3), the localization of P41 and P24 was unknown. For these experiments, we introduced a second fluorescent protein, ECFP (a blue-colored derivative of GFP) (10), to mark the positions of the attachment organelles of living cells. The *ecfp* gene was fused to the 5' end of the *p65* gene and was under the control of the *tuf* promoter. This *ecfp-p65* fusion gene was introduced into *M. pneumoniae* M129 by use of a Cm^r derivative of Tn4001mod (11) (Fig. 1B). The resulting Cm^r transformant, which we designated TK210, expressed ECFP-P65 at a level slightly lower than that of native P65 (Fig. 5A) and exhibited blue fluorescent signals at the cell poles (attachment organelle) (Fig. 5B). We used TK210 as a host strain to examine the subcellular localization of HMW2, P41, and P24.

We constructed two groups of plasmids for the expression of EYFP fusions of HMW2, P41, and P24 by modifying plasmids pTK164 and pTK165 (Table 3). The first group of plasmids was designated pMPN (derivatives of pTK164); each of these plasmids possessed the *eyfp-hmw2*, *eyfp-p41*, or *eyfp-p24* fusion genes under the control of the *p65* promoter for low-level expression (Table 3). The second group of plasmids, designated pMPN-tuf (derivatives of pTK165) (Table 3), contained the *eyfp-hmw2*, *eyfp-p41*, or *eyfp-p24* fusion genes under the control of the *tuf* promoter for high-level expression. These plasmids were introduced into strain TK210, and Cm^r - Gm^r transformants were obtained. Western blot analysis for the fusion proteins confirmed that transformants TK2310, TK2311, and TK2312 (created with pMPN plasmids) expressed EYFP-HMW2, EYFP-P41, and EYFP-P24 at low levels (Fig. 6A), while transformants TK2310T, TK2311T, and TK2312T (created with pMPN-tuf plasmids) expressed them at higher levels (Fig. 6B). The EYFP fluorescent signals of strains with low-level expression were weak and were captured with an exposure time longer than that of strains with high-level expression (Fig. 7).

Strains TK2310 and TK2310T expressing EYFP-HMW2 showed fluorescent signals for EYFP at their cell poles. The distribution patterns for fluorescent foci were basically identical between the two strains, regardless of the level of expression of EYFP-HMW2, but the fluorescence signal intensities reflected the expression levels, as indicated by the difference in brightness between the focus signals and the background of the EYFP images (Fig. 7). In both strains, the fluorescent foci of EYFP-HMW2 almost overlapped those of ECFP-P65 (Fig. 7), indicating that the HMW2 protein was localized at the attachment organelle. These results confirmed the findings of Balish et al. (3).

Transformants TK2311, TK2312, TK2311T, and TK2312T revealed that EYFP-P41 and EYFP-P24 formed fluorescent foci in *M. pneumoniae* cells (Fig. 7). Unlike EYFP-HMW2, the

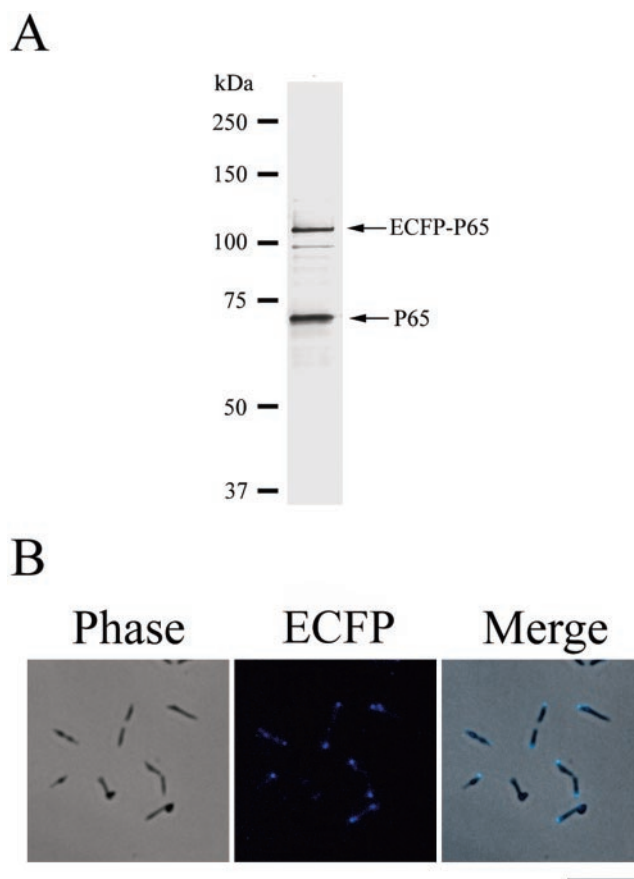


FIG. 5. Western blot analysis and fluorescence microscopy of *M. pneumoniae* TK210. (A) Western blot analysis of *M. pneumoniae* strain TK210. Lysates of *M. pneumoniae* TK210 cells (5 μg of total protein) were separated by SDS-8% PAGE, transferred to a nitrocellulose membrane, and probed with an anti-P65 antibody. The positions of the detected ECFP-P65 and native P65 are indicated by arrows. Molecular sizes are shown at left. (B) Subcellular localization of the ECFP-P65 fusion. The left and middle panels show the same cells observed by phase-contrast microscopy and fluorescence microscopy, respectively. The right panel shows the merged image of the left and middle panels. Bar, 5 μm .

foci of EYFP-P41 and EYFP-P24 were located mainly at the proximal region of the attachment organelle and did not overlap those of ECFP-P65. In strains showing low-level expression of EYFP-P41 or EYFP-P24 (TK2311 and TK2312), the fluorescent foci of these proteins were confined to the proximal end of the attachment organelle (Fig. 7), and the profiles of these proteins were very similar. However, in strains showing high-level expression (TK2311T and TK2312T), the distribution patterns for fluorescent signals were not identical between EYFP-P41 and EYFP-P24 (Fig. 7). In strain TK2311T, additional fluorescent foci for EYFP-P41 were frequently observed at the opposite end of the attachment organelle, i.e., at the cell tail (Fig. 7). On the other hand, the fluorescence signals for EYFP-P24 were diffused from the proximal end of the organelle to the cell tail (Fig. 7, TK2312T). These nonidentical distribution patterns for EYFP-P41 and EYFP-P24 in strains showing high-level expression suggested that these proteins had different properties in the cells. However, even in these strains showing high-level expression, the strongest signals

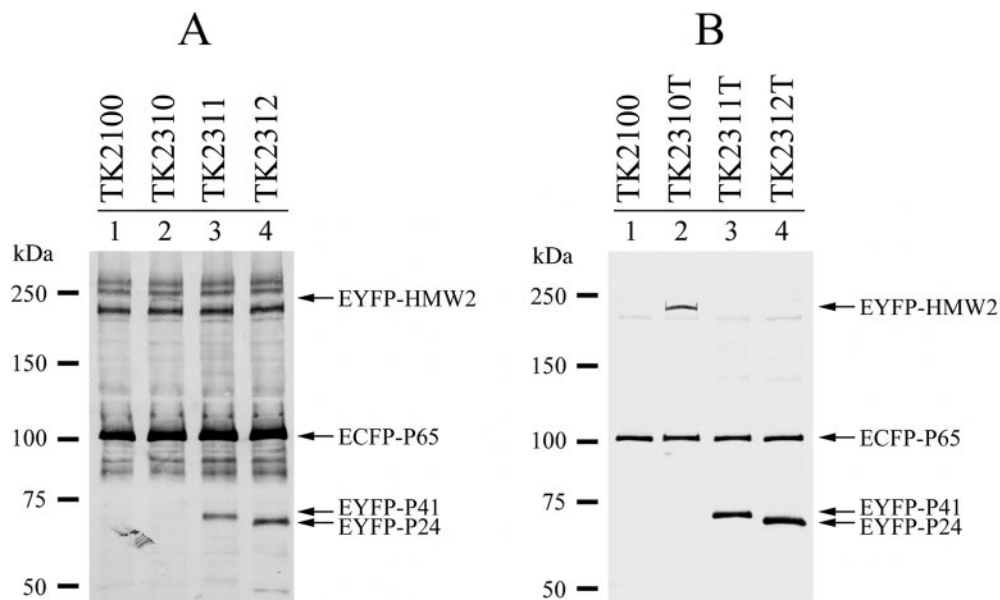


FIG. 6. Expression of EYFP-HMW2, EYFP-P41, and EYFP-P24 fusions in *M. pneumoniae* cells. (A) Western blot analysis of low-level expression transformants of EYFP fusions. Lysates of *M. pneumoniae* transformant cells (TK2100, TK2310, TK2311, and TK2312) (10 μ g of total protein) were separated by SDS-5 to 10% gradient PAGE, transferred to a nitrocellulose membrane, and probed with an anti-GFP variant antibody. The positions of detected EYFP-HMW2, EYFP-P41, EYFP-P24, and ECFP-P65 are indicated by arrows. Molecular sizes are shown at left. (B) Western blot analysis of high-level expression transformants. Lysates of *M. pneumoniae* transformant cells (TK2100, TK2310T, TK2311T, and TK2312T) (5 μ g of total protein) were analyzed under the same conditions in those used in panel A. The positions of detected fusion proteins are indicated by arrows.

were located at the proximal end of the organelle, suggesting that this site is the preferential localization site for both P41 and P24.

We also transformed *M. pneumoniae* M129 with the pMPN and pMPN-tuf plasmids, and the *eyfp-hmw2*, *eyfp-p41*, and *eyfp-p24* fusion genes were expressed (strains TK3310, TK3311, TK3312, TK3310T, TK3311T, and TK3312T). We confirmed that the localization patterns for EYFP-HMW2, EYFP-P41, and EYFP-P24 in the background of strain M129 were identical to those in the background of strain TK210 (Fig. 8A; only the images for TK3310T, TK3311T, and TK3312T are shown); these results indicate that the presence of ECFP-P65 does not affect the localization of these EYFP fusions.

DISCUSSION

Fluorescent-protein tagging is a widely used strategy for visualizing proteins in living cells. In this study, we have constructed vectors for fluorescent-protein tagging in *M. pneumoniae* and used them to visualize the protein components of cytoskeleton-like structures. The vectors constructed in this study are based on the Tn4001mod vector system (11, 22) and possess *M. pneumoniae* *p65* or *tuf* promoters for the expression of fluorescent target proteins. These two promoters allow for high and low levels of expression of target proteins and are helpful for enhancing the resolution of fluorescent images and assessing the patterns of localization of target proteins. We used EYFP and ECFP as fluorescent-protein tags and designed a coexpression procedure for these proteins. This procedure enabled dual labeling of two target proteins in living *M. pneumoniae* cells. Since *M. pneumoniae* cells are pleomorphic,

it is sometimes difficult to judge the position of the attachment organelle in the cell. The dual-labeling method made it easier to ascertain the position of the organelle relative to the target protein. The first fluorescent protein can be used to label the organelle, while the second is used for the other target proteins.

Using our fluorescent-protein tagging method, we visualized the four proteins—P65, HMW2, P41, and P24—that are encoded in the *crl* operon (Fig. 1A). The P65 protein labeled with EYFP was localized at the attachment organelle (Fig. 2), confirming previous observations obtained by immunofluorescence microscopy (20, 48, 49). The localization of P65 at the organelle indicates that P65 is a component of the attachment organelle. However, neither the function of P65 nor its involvement in cytodherence is fully understood, mainly because of the lack of P65 mutant strains. It is known that P65 is present at reduced steady-state levels in mutant strains that lack any of the cytodherence accessory proteins—HMW1, HMW2, HMW3, and P30. In these mutant strains, the polar localization of P65 is partially disrupted, depending on the extent to which the P65 levels are reduced (2, 20, 52). The stability and polar localization of P65 are thought to be correlated. To stabilize P65, it may be necessary to incorporate it into the stable localization site at the organelle. This stable localization site may be provided by the other cytoskeletal proteins (25). Unincorporated P65 tends to be degraded by proteolysis. Consistent with this model, in strain TK162, expressing a high level of EYFP-P65, the level of native P65 was lower than the levels in the other strains (Fig. 3, lane 4). It is likely that the localization site for P65 at the organelle was occupied by an excess of EYFP-P65 in this strain and that unincorporated native P65 and EYFP-P65 were degraded. This sce-

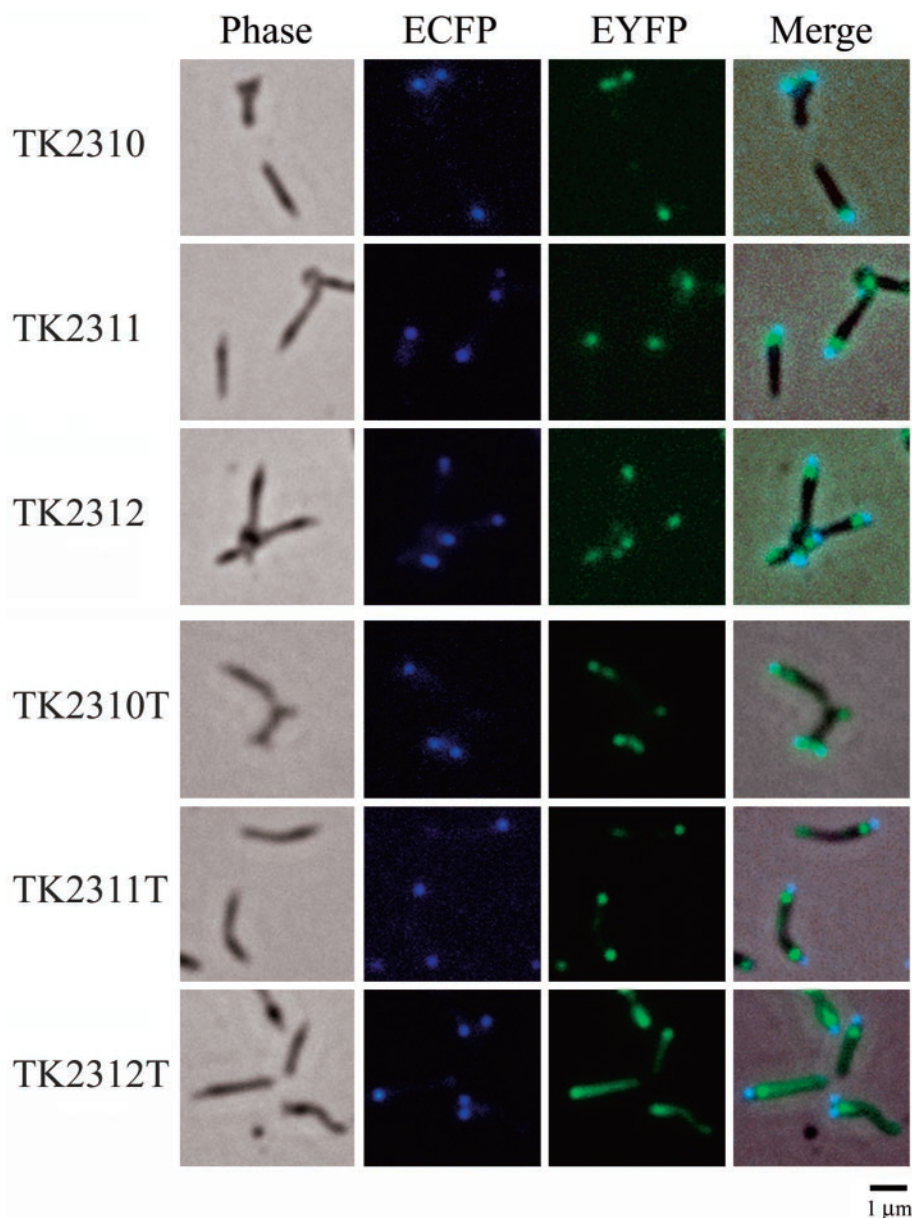


FIG. 7. Subcellular localization of EYFP-HMW2, EYFP-P41, and EYFP-P24 fusions in the *M. pneumoniae* TK210 cell background. Images of six *M. pneumoniae* transformants (names at left) are shown. The first panel in each row shows the phase-contrast image of the cells. The second and third panels in each row show ECFP and EYFP fluorescence images of the same cells, respectively. The fourth panel in each row shows the merged image of the phase-contrast and fluorescence images. Transformants TK2310, TK2311, and TK2312 show low levels of expression of EYFP-HMW2, EYFP-P41, and EYFP-P24, respectively; transformants TK2310T, TK2311T, and TK2312T show high levels of expression. Bar, 1 μm .

nario may also explain the clear focal fluorescence signals of EYFP-P65 at the attachment organelle and the lesser amounts of additional fluorescence in other parts of *M. pneumoniae* cells, even with high-level expression of EYFP-P65 (Fig. 2). Because EYFP-P65 gave clear focal fluorescence signals at the organelle, we also labeled P65 with ECFP and used ECFP-P65 as a positional marker of the organelle for examining the localizations of the other proteins (Fig. 5).

The HMW2 protein is a critical factor for cytoadherence. It is thought to function in the early stage of assembly of the attachment organelle, together with the HMW1 protein (25). The loss of HMW2 affects the stability and polar localization of

most of the other cytoadherence accessory proteins, but HMW2 itself is also less stable in the absence of HMW1 (2). The EYFP-HMW2 fusion was localized at the attachment organelle when expressed at both high and low levels (Fig. 7), supporting the observations of Balish et al. (3). The localization sites for EYFP-HMW2 were almost identical to those for ECFP-P65 coexpressed in the same cells. However, in a considerable number of these cells, the fluorescence signals from EYFP-HMW2 extended slightly farther toward the proximal end than did the signals from ECFP-P65, which were relatively limited to the distal end of the organelle (data not shown). These observations agree with previous ones (49) and with the cur-

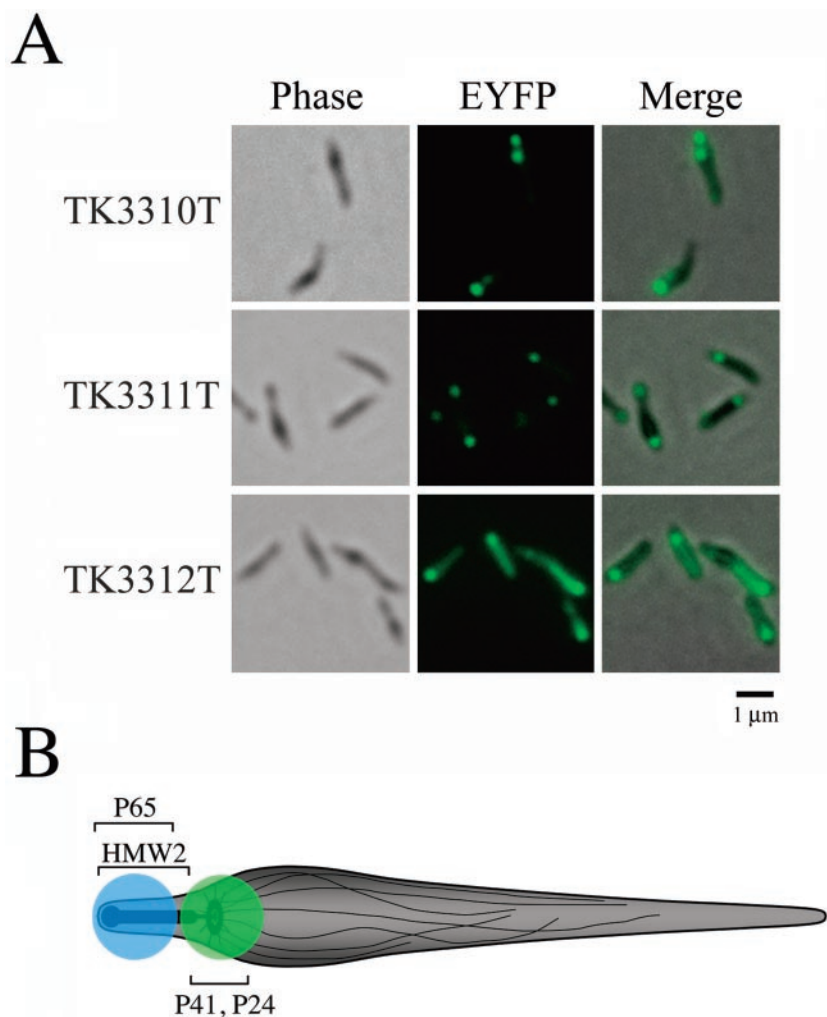


FIG. 8. (A) Subcellular localization of EYFP-HMW2, EYFP-P41, and EYFP-P24 fusions in the wild-type *M. pneumoniae* M129 cell background (without ECFP-P65). The left and middle panels in each row show images of the same cells observed by phase-contrast microscopy and fluorescence microscopy, respectively. The right panel in each row shows the merged image of the left and middle panels. The transformants are named at left. Bar, 1 μm. (B) Schematic illustration of an *M. pneumoniae* cell. Cytoskeleton-like structures within the *M. pneumoniae* cell (electron-dense core, wheel-like structure, and fibrous network) are illustrated (see the text). Approximate positions of the fluorescent signals observed by microscopy are shown with colors (blue, ECFP-P65; green, EYFP-P41 and EYFP-P24). Positions of sites of localization of P65, HMW2, P41, and P24 are indicated.

rent structural model of the organelle, which proposes that P65 is localized at the surface of the distal end of the attachment organelle and that HMW2 is the most probable component of the electron-dense core (25).

Little is known about the P41 and P24 proteins (25, 28). A homologous gene for P41 is present in the closely related species *Mycoplasma genitalium* (17), but no homologous gene has been found for P24. Although the functions of P41 and P24 are unknown, both attract considerable interest as cytoskeletal proteins, since they are encoded in the *crl* operon, together with P65 and HMW2, and are associated with the Triton shell (H. Ogaki et al., unpublished data). In addition, the P41 protein is predicted to contain a coiled-coil structure that has been observed in the other cytoskeletal proteins. Therefore, we analyzed the subcellular localization of these proteins by fluorescent-protein tagging and demonstrated that EYFP-P41 and EYFP-P24 were preferentially localized at the proximal end of

the attachment organelle in *M. pneumoniae* cells, suggesting that they are cytoskeletal proteins that form unknown structures at this site. However, it should be noted that the high-level expression of both of these proteins exhibited additional fluorescent signals in the cells (Fig. 7). We thought that these additional localization patterns were caused by accumulations of excess proteins in the cells, but it remains possible that these localization patterns in cells with high-level expression reflect the native localization patterns for P41 and P24. This point must be assessed by using another method, such as immunofluorescence. If P41 and P24 really do localize to the proximal end of the attachment organelle, then what structures are present at this site? Recently, the presence of a wheel-like complex that might be part of a cytoskeleton-like structure was suggested at the proximal end of the electron-dense core by transmission electron microscopy of an ultrathin section of *M. pneumoniae* cells (16). This wheel-like complex is structurally

similar to the flagellar motor and might be connected to fibrous structures extending into the cytoplasm of *M. pneumoniae* cells. The detailed structure of this wheel-like complex has yet to be elucidated, but its position (at the proximal end of the electron-dense core) corresponds to the P41 and P24 localization site (Fig. 8B).

We also used the fluorescent-protein tagging technique to observe gliding *M. pneumoniae* cells (Fig. 4). The expression of EYFP-P65 in *M. pneumoniae* allowed real-time visualization of the attachment organelle of gliding cells by phase-contrast and fluorescence microscopy. The successful labeling of the attachment organelle of living *M. pneumoniae* cells indicated that this technique should be applicable to the direct observation of the cell division processes in *M. pneumoniae* (i.e., nascent organelle formation, the migration of one of the organelles to the opposite end, and cytokinesis) (34, 36, 48). However, an attempt at such an application was not successful in this study. The major reason for this result might have been the nutrient conditions of *M. pneumoniae* cells used for microscopy. We used saline containing 20% horse serum to suspend cells for fluorescence microscopy in order to reduce background fluorescence. Such low-nutrient conditions might not be sufficient to support cell division in *M. pneumoniae*. If cell division did somehow occur under these conditions, then a longer observation time might have been required, since the doubling time of *M. pneumoniae* M129 is estimated to be about 10 h, even under optimal conditions (31). In future studies, these situations could be improved by reducing the background fluorescence in the medium or by using fusion proteins with more intense signals.

ACKNOWLEDGMENTS

We are grateful to D. C. Krause of the University of Georgia for providing plasmid pKV104 and to C. Citti of the University of Veterinary Medicine, Vienna, Austria, for providing plasmid pISM2062.2. We thank Y. Arakawa of the National Institute of Infectious Diseases, Tokyo, Japan, for helpful input.

This work was supported in part by a Grant-in-Aid for JSPS Fellows from the Japan Society for the Promotion of Science (to S.S.) and by Grants-in-Aid for Young Scientists (to A.H.), for Scientific Research (to M.M.), and for Science Research on Priority Areas (motor proteins, genome science, and infection and host response) (to M.M.) from the Ministry of Education, Culture, Sports, Science, and Technology of Japan.

REFERENCES

1. Aluotto, B. B., R. G. Wittler, C. O. Williams, and J. E. Faber. 1970. Standardized bacteriologic techniques for the characterization of mycoplasma species. *Int. J. Syst. Bacteriol.* **20**:35–58.
2. Balish, M. F., and D. C. Krause. 2002. Cytadherence and cytoskeleton, p. 491–518. *In* S. Razin and R. Herrmann (ed.), *Molecular biology and pathogenicity of mycoplasmas*. Kluwer Academic/Plenum Publishers, New York, N.Y.
3. Balish, M. F., R. T. Santurri, A. M. Ricci, K. K. Lee, and D. C. Krause. 2003. Localization of *Mycoplasma pneumoniae* cytodherence-associated protein HMW2 by fusion with green fluorescent protein: implications for attachment organelle structure. *Mol. Microbiol.* **47**:49–60.
4. Berg, H. C., and L. Turner. 1993. Torque generated by the flagellar motor of *Escherichia coli*. *Biophys. J.* **65**:2201–2216.
5. Biberfeld, G., and P. Biberfeld. 1970. Ultrastructural features of *Mycoplasma pneumoniae*. *J. Bacteriol.* **102**:855–861.
6. Brecht, W. 1968. Motility and multiplication of *Mycoplasma pneumoniae*. A phase contrast study. *Pathol. Microbiol. (Basel)* **32**:321–326.
7. Brecht, W. 1973. Motility of mycoplasmas. *Ann. N. Y. Acad. Sci.* **225**:246–250.
8. Dandekar, T., M. Huynen, J. T. Regula, B. Ueberle, C. U. Zimmermann, M. A. Andrade, T. Doerks, L. Sanchez-Pulido, B. Snel, M. Suyama, Y. P. Yuan, R. Herrmann, and P. Bork. 2000. Re-annotating the *Mycoplasma pneumoniae* genome sequence: adding value, function and reading frames. *Nucleic Acids Res.* **28**:3278–3288.
9. Feldner, J., U. Gobel, and W. Brecht. 1982. *Mycoplasma pneumoniae* adhesin localized to tip structure by monoclonal antibody. *Nature* **298**:765–767.
10. Green, G., S. R. Kain, and B. Angres. 2000. Dual color detection of cyan and yellow derivatives of green fluorescent protein using conventional fluorescence microscopy and 35-mm photography. *Methods Enzymol.* **327**:89–94.
11. Hahn, T. W., E. A. Mothershed, R. H. Waldo, and D. C. Krause. 1999. Construction and analysis of a modified Tn4001 conferring chloramphenicol resistance in *Mycoplasma pneumoniae*. *Plasmid* **41**:120–124.
12. Hahn, T. W., M. J. Wilby, and D. C. Krause. 1998. HMW1 is required for cytodhesin P1 trafficking to the attachment organelle in *Mycoplasma pneumoniae*. *J. Bacteriol.* **180**:1270–1276.
13. Hanahan, D. 1983. Studies on transformation of *Escherichia coli* with plasmids. *J. Mol. Biol.* **166**:557–580.
14. Hansen, E. J., R. M. Wilson, and J. B. Baseman. 1979. Isolation of mutants of *Mycoplasma pneumoniae* defective in hemadsorption. *Infect. Immun.* **23**:903–906.
15. Hedreyda, C. T., K. K. Lee, and D. C. Krause. 1993. Transformation of *Mycoplasma pneumoniae* with Tn4001 by electroporation. *Plasmid* **30**:170–175.
16. Hegermann, J., R. Herrmann, and F. Mayer. 2002. Cytoskeletal elements in the bacterium *Mycoplasma pneumoniae*. *Naturwissenschaften* **89**:453–458.
17. Himmelreich, R., H. Plagens, H. Hilbert, B. Reiner, and R. Herrmann. 1997. Comparative analysis of the genomes of the bacteria *Mycoplasma pneumoniae* and *Mycoplasma genitalium*. *Nucleic Acids Res.* **25**:701–712.
18. Hu, P. C., R. M. Cole, Y. S. Huang, J. A. Graham, D. E. Gardner, A. M. Collier, and W. A. Clyde, Jr. 1982. *Mycoplasma pneumoniae* infection: role of a surface protein in the attachment organelle. *Science* **216**:313–315.
19. Inamine, J. M., S. Loechel, and P. C. Hu. 1988. Analysis of the nucleotide sequence of the P1 operon of *Mycoplasma pneumoniae*. *Gene* **73**:175–183.
20. Jordan, J. L., K. M. Berry, M. F. Balish, and D. C. Krause. 2001. Stability and subcellular localization of cytodherence-associated protein P65 in *Mycoplasma pneumoniae*. *J. Bacteriol.* **183**:7387–7391.
21. Kirchoff, H. 1992. Motility, p. 473–489. *In* J. Maniloff, R. N. McElhaney, L. R. Finch, and J. B. Baseman (ed.), *Mycoplasmas: molecular biology and pathogenesis*. American Society for Microbiology, Washington, D.C.
22. Knudtson, K. L., and F. C. Minion. 1993. Construction of Tn4001lac derivatives to be used as promoter probe vectors in mycoplasmas. *Gene* **137**:217–222.
23. Krause, D. C. 1998. *Mycoplasma pneumoniae* cytodherence: organization and assembly of the attachment organelle. *Trends Microbiol.* **6**:15–18.
24. Krause, D. C. 1996. *Mycoplasma pneumoniae* cytodherence: unravelling the tie that binds. *Mol. Microbiol.* **20**:247–253.
25. Krause, D. C., and M. F. Balish. 2004. Cellular engineering in a minimal microbe: structure and assembly of the terminal organelle of *Mycoplasma pneumoniae*. *Mol. Microbiol.* **51**:917–924.
26. Krause, D. C., and M. F. Balish. 2001. Structure, function, and assembly of the terminal organelle of *Mycoplasma pneumoniae*. *FEMS Microbiol. Lett.* **198**:1–7.
27. Krause, D. C., D. K. Leith, R. M. Wilson, and J. B. Baseman. 1982. Identification of *Mycoplasma pneumoniae* proteins associated with hemadsorption and virulence. *Infect. Immun.* **35**:809–817.
28. Krause, D. C., T. Proft, C. T. Hedreyda, H. Hilbert, H. Plagens, and R. Herrmann. 1997. Transposon mutagenesis reinforces the correlation between *Mycoplasma pneumoniae* cytoskeletal protein HMW2 and cytodherence. *J. Bacteriol.* **179**:2668–2677.
29. Layh-Schmitt, G., and R. Herrmann. 1992. Localization and biochemical characterization of the ORF6 gene product of the *Mycoplasma pneumoniae* P1 operon. *Infect. Immun.* **60**:2906–2913.
30. Layh-Schmitt, G., A. Podtelejnikov, and M. Mann. 2000. Proteins complexed to the P1 adhesin of *Mycoplasma pneumoniae*. *Microbiology* **146**:741–747.
31. Lipman, R. P., W. A. Clyde, Jr., and F. W. Denny. 1969. Characteristics of virulent, attenuated, and avirulent *Mycoplasma pneumoniae* strains. *J. Bacteriol.* **100**:1037–1043.
32. McBride, M. J. 2001. Bacterial gliding motility: multiple mechanisms for cell movement over surfaces. *Annu. Rev. Microbiol.* **55**:49–75.
33. Meng, K. E., and R. M. Pfister. 1980. Intracellular structures of *Mycoplasma pneumoniae* revealed after membrane removal. *J. Bacteriol.* **144**:390–399.
34. Miyata, M. 2002. Cell division, p. 117–130. *In* S. Razin and R. Herrmann (ed.), *Molecular biology and pathogenicity of mycoplasmas*. Kluwer Academic/Plenum Publishers, New York, N.Y.
35. Miyata, M., W. S. Ryu, and H. C. Berg. 2002. Force and velocity of *Mycoplasma mobile* gliding. *J. Bacteriol.* **184**:1827–1831.
36. Miyata, M., and S. Seto. 1999. Cell reproduction cycle of mycoplasma. *Biochimie* **81**:873–878.
37. Miyata, M., and A. Uenoyama. 2002. Movement on the cell surface of the gliding bacterium, *Mycoplasma mobile*, is limited to its head-like structure. *FEMS Microbiol. Lett.* **215**:285–289.
38. Miyata, M., H. Yamamoto, T. Shimizu, A. Uenoyama, C. Citti, and R. Rosengarten. 2000. Gliding mutants of *Mycoplasma mobile*: relationships

- between motility and cell morphology, cell adhesion and microcolony formation. *Microbiology* **146**:1311–1320.
39. **Phillips, G. J.** 2001. Green fluorescent protein—a bright idea for the study of bacterial protein localization. *FEMS Microbiol. Lett.* **204**:9–18.
40. **Proft, T., H. Hilbert, G. Layh-Schmitt, and R. Herrmann.** 1995. The proline-rich P65 protein of *Mycoplasma pneumoniae* is a component of the Triton X-100-insoluble fraction and exhibits size polymorphism in the strains M129 and FH. *J. Bacteriol.* **177**:3370–3378.
41. **Proft, T., H. Hilbert, H. Plagens, and R. Herrmann.** 1996. The P200 protein of *Mycoplasma pneumoniae* shows common features with the cytodherence-associated proteins HMW1 and HMW3. *Gene* **171**:79–82.
42. **Radestock, U., and W. Bredt.** 1977. Motility of *Mycoplasma pneumoniae*. *J. Bacteriol.* **129**:1495–1501.
43. **Razin, S., and E. Jacobs.** 1992. Mycoplasma adhesion. *J. Gen. Microbiol.* **138**:407–422.
44. **Razin, S., D. Yogeve, and Y. Naot.** 1998. Molecular biology and pathogenicity of mycoplasmas. *Microbiol. Mol. Biol. Rev.* **62**:1094–1156.
45. **Regula, J. T., G. Boguth, A. Gorg, J. Hegermann, F. Mayer, R. Frank, and R. Herrmann.** 2001. Defining the mycoplasma 'cytoskeleton': the protein composition of the Triton X-100 insoluble fraction of the bacterium *Mycoplasma pneumoniae* determined by 2-D gel electrophoresis and mass spectrometry. *Microbiology* **147**:1045–1057.
46. **Romero-Arroyo, C. E., J. Jordan, S. J. Peacock, M. J. Willby, M. A. Farmer, and D. C. Krause.** 1999. *Mycoplasma pneumoniae* protein P30 is required for cytodherence and associated with proper cell development. *J. Bacteriol.* **181**:1079–1087.
47. **Sambrook, J., and D. W. Russell.** 2001. *Molecular cloning: a laboratory manual*, 3rd ed. Cold Spring Harbor Laboratory Press, Cold Spring Harbor, N.Y.
48. **Seto, S., G. Layh-Schmitt, T. Kenri, and M. Miyata.** 2001. Visualization of the attachment organelle and cytodherence proteins of *Mycoplasma pneumoniae* by immunofluorescence microscopy. *J. Bacteriol.* **183**:1621–1630.
49. **Seto, S., and M. Miyata.** 2003. Attachment organelle formation represented by localization of cytodherence proteins and formation of the electron-dense core in wild-type and mutant strains of *Mycoplasma pneumoniae*. *J. Bacteriol.* **185**:1082–1091.
50. **Southward, C. M., and M. G. Surette.** 2002. The dynamic microbe: green fluorescent protein brings bacteria to light. *Mol. Microbiol.* **45**:1191–1196.
51. **Stevens, M. K., and D. C. Krause.** 1991. Localization of the *Mycoplasma pneumoniae* cytodherence-accessory proteins HMW1 and HMW4 in the cytoskeletonlike Triton shell. *J. Bacteriol.* **173**:1041–1050.
52. **Willby, M. J., and D. C. Krause.** 2002. Characterization of a *Mycoplasma pneumoniae hmw3* mutant: implications for attachment organelle assembly. *J. Bacteriol.* **184**:3061–3068.
53. **Yanisch-Perron, C., J. Vieira, and J. Messing.** 1985. Improved M13 phage cloning vectors and host strains: nucleotide sequences of the M13mp18 and pUC19 vectors. *Gene* **33**:103–119.